SCHLIEREN VISUALIZATIONS OF NON-IDEAL COMPRESSIBLE FLUID FLOWS

Conti C.C.[1], Spinelli A.[1], Cammi G.[1], Zocca M.[2], Cozzi F.[1], Guardone A.[2].
[1] Energy Department, [2] Aerospace Science and Technology Department
Politecnico di Milano
Milan, Italy
E-mail: camillacecilia.conti@mail.polimi.it

ABSTRACT

The peculiarities of schlieren visualizations of non-ideal compressible fluid flows are analyzed with the support of experimental evidence and numerical calculation. Schlieren visualizations are performed on a vapor flow of Siloxane MDM (Octamethyltrisiloxane, $C_8H_{24}O_2Si_3$) expanding to supersonic speeds, up to a Mach number of 2, within a converging-diverging nozzle. The nozzle constitutes the test section of the Test Rig for Organic Vapors (TROVA), an experimental facility built at the Laboratory of Compressible fluid dynamics for Renewable Energy Applications (CREA Lab) of Politecnico di Milano (Italy) to investigate non-ideal expansions of complex organic vapors close to the saturation curve and the critical point, representative of blade channel flows in Organic Rankine Cycle (ORC) turbines. The schlieren system used in this work employs a double-pass configuration featuring a mercury lamp, a bi-convex lens, a cubic beam splitter, a second focusing lens and a high-speed CMOS camera. Visualizations of MDM vapor flows showed measuring-range issues: portions of the image expected to appear bright due to negative density gradients (expansion), were dark instead. This was attributed to the strong density gradients occurring in these non-ideal flows, causing refractions intense enough to deflect light onto some system aperture stop. Ray tracing calculation indeed showed that rays crossing regions of the test area with stronger gradients were intercepted by the knife frame before reaching the camera sensor. Interestingly, these measuring range issues were found to decrease as the non-ideality of the flow decreased. Moreover, when the same nozzle geometry was used for analogous testing with air, these measuring-range issues were absent or noticeably reduced. This paper analyses both experimental and numerical evidence to investigate the two aforementioned observations and provide an explanation in terms of refractive index gradient, compressibility and pressure ratio gradient trends during an expansion.

INTRODUCTION

Non-ideal compressible fluid dynamics is a branch of gas-dynamics drawing increasing interest due to the number of industrial processes involving such flows. In the power production field, non-ideal gas flows occur in Organic Rankine Cycles (ORCs). They are preferred to conventional steam cycles when low to medium source temperature and low to medium power output are considered, thanks to their low cost, plant simplicity and thermodynamic efficiency. Fluids usually employed in ORCs feature high complexity and molecular weight, and turbine expansion occurs in the dense gas region (near the saturation curve and the critical point). As a result, turbine flows are highly supersonic and show non-neglible real gas effects, requiring accurate design tools accounting for these aspects in order to achieve high turbine efficiency, which in turn strongly impacts cycle efficiency [1,2].

Experimental data is needed for flow characterization and for the validation of design tools, including thermodynamic models. This is why the *Test Rig for Organic Vapors* (TROVA) was built at the Laboratory of Compressible fluid dynamics for Renewable Energy Applications (CREA Lab) of Politecnico di Milano [3]. The employed fluid is Siloxane MDM (Octamethyltrisiloxane, $C_8H_{24}O_2Si_3$), a silicon oil of particular interest for high temperature ORC applications. Independent temperature and pressure measurements are performed on non-ideal flows expanding in a nozzle test section and schlieren visualizations are employed to help the understanding of the occuring gas-dynamic phenomena. Schlieren images of MDM vapor flows display measuring-range

NOMENCLATURE

P	[bar]	Pressure
T	[°C]	Temperature
Z	[-]	Compressibility Factor
f	[mm]	Lens focal length
d	[mm]	Lens diameter
n	[-]	Refractive index
K	$[m^3/kg]$	Gladstone-Dale coefficient
ε	[rad]	Angular ray deflection
L	[m]	Depth of test section
ρ	$[kg/m^3]$	Density
c	$[m/s]$	Speed of Sound
$\frac{1}{c^2}$	$[s^2/m^2]$	Compressibility
$\mathcal{R}$	[J/mol/K]	Universal Gas Constant
M_m	[kg/kmol]	Molar Mass
γ	[-]	Specific heat ratio
M	[-]	Mach Number

Special characters

ρ	$[kg/m^3]$	Density

Subscripts

T	Total conditions
0	Reference conditions
∞	Undisturbed conditions (inlet of test section)

issues: portions of the image corresponding to expansion fans appear dark instead of being bright, as it would be expected from the chosen knife position. This kind of measuring range issue decreases as the non-ideality of the flow decreases. Also, when air was used during preliminary TROVA experiments, these issues were much less noticeable. In order to explain these two observations, an analytical expression for the refractive index gradient in terms of notable thermodynamic quantities is derived. The role played by each parameter is investigated with the help of numerical simulations. To specifically identify the effect of the flow non-ideality and provide general results for schlieren visualizations of non-ideal flows, both polytropic ideal gas and real gas simulations are looked at.

The present paper is structured as follows. The EXPERIMENTAL SETUP section describes the TROVA and the employed optical bench. An explanation of the experimental results, data elaboration and analysis is then provided in EXPERIMENTAL RESULTS, followed by CONCLUSIONS on the impact of the analysed parameters on schlieren imaging.

EXPERIMENTAL SETUP

The TROVA

The *Test Rig for Organic VApors* (TROVA), located at the CREAlab of Politecnico di Milano, is an experimental apparatus designed to investigate real gas effects occurring in turbine flows of organic vapors. The TROVA operates as a blow-down wind tunnel based on an ORC, where the turbine is replaced by a planar straight-axis converging-diverging nozzle - the simplest geometry representative of turbine blade channels [3].

The nozzle is designed with the standard method of characteristics [4] combined with the Span-Wagner thermodynamic model [5] embedded in the *FluidProp* ® software [6] to obtain a uniform flow at the outlet with Mach number $M = 2$. The nozzle operates in underexpanded conditions, thus exhibiting a large isentropic core: fields of thermodynamic quantities can be derived from simultaneous total temperature T_T and pressure P_T measures at the nozzle inlet and from static pressure measurements P_i (i=pressure tap number) along the nozzle axis. Since the flow is isentropic, $s_i = s_0 = s(P_T, T_T)$: thus, any thermodynamic quantity along the nozzle can be calculated using a suitable thermodynamic model as a function of the local measured pressure P_i and the entropy s_i (for example, $h_i = h(P_i, s_i)$ is the enthalpy).

The working fluid employed in this work is Siloxane MDM: its thermodynamic properties are calculated with the use of the Span-Wagner model.

The implemented batch thermodynamic cycle is shown in Figure 1. The required amount of fluid is stored and isochorically heated to the desired temperature and pressure in a closed volume to superheated conditions ($2 \rightarrow 6$). The fluid flows through a plenum upstream of the nozzle, where total pressure P_{T6} and total temperature T_{T6} are measured. No stagnation pressure regulation occurs, so total pressure decreases in time due to emptying of the tank. The fluid expands through the planar nozzle ($6 \rightarrow 7$), and static pressures along the axis are measured. The flow is then slowed down to rest ($7 \rightarrow 8$), de-superheated ($8 \rightarrow 9$) and condensed ($9 \rightarrow 1$) with isochoric processes in a low pressure vessel. A metering pump compresses the liquid back to the high pressure vessel ($1 \rightarrow 2$).

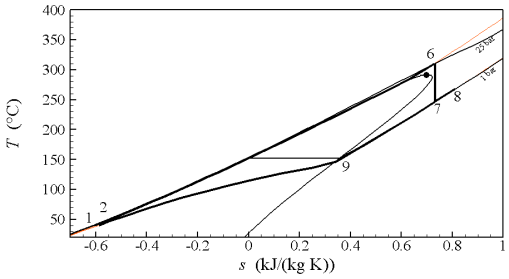

Figure 1. Thermodynamic cycle implemented by the TROVA. Thin red lines are isochores; thin black lines are isobars and saturation curves; thick black lines represent the cycle.

Fluid	**Test Name**	Z_T	P_T $[bar]$	T_T $[°C]$
MDM, *Test04*	MDM_a	0.82	4.58	246
	MDM_b	0.85	3.98	249
	MDM_c	0.88	3.38	250
	MDM_d	0.93	1.80	232
	MDM_e	0.97	0.62	226
Air	Air	1.00	4.00	40

Table 1. Summary of the test conditions analysed in this paper.

Stagnation conditions upstream of the nozzle are chosen so that dense-gas regions can be explored during the expansion and flows of interest for ORCs can be investigated. *Test04*, representative of all experimental tests performed, is considered for analysis. Due to the discharge of the high pressure vessel during the test and the lack of pressure regulation at the nozzle inlet, different total conditions can be investigated in one single experimental run, as reported in Table 1. Total pressure decreases in time as the test proceeds, correponding to an increasing compressibility factor and to a lower degree of non-ideality in the initial vapor conditions. Experimental data and schlieren images are extracted from primary data at the minimum and maximum total Z values upstream of the nozzle and at evenly spaced values in between. Data relative to a preliminary experimental run with air is also reported. This set of results provides the ground for analysis in this paper.

The MDM_{M2} nozzle geometry, employed in this work, is characterized by the presence of a step at the throat (at coordinate $x/H \simeq 10.29$) to fix the location of the minimum nozzle area, independently from boundary layer unsteadiness [7]. Complex flow features originate at the step position and propagate along the nozzle. A representative experimental schlieren image is found in Figure 2. An expansion fan is present at the step edge (point A), followed by an oblique shock at the reattachment point downstream of point B: the latter occurs at a Mach number only

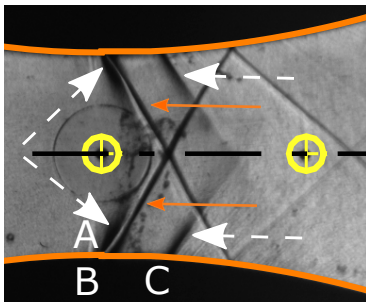

Figure 2. Enlargement at the throat region of the schlieren image of MDM_d, annotated with the flow structures due to the step. A,B and C are the step edges. The white dashed arrows indicate the expansion fans whilst the orange solid arrows indicate oblique shocks. Due to measuring range issues, expansion fans are dark instead of being bright.

slightly larger than 1 and is thus very weak, resulting in negligible entropy production (the flow can thus still be considered as isentropic). A second expansion fan occurs where the plateau of the recessed step ends and the nozzle curvature begins (point C). The two expansion fans are the object of the measuring range issues considered in this paper.

The Schlieren Bench

The optical bench for schlieren visualizations schematized in Figure 3 employs a double-pass configuration.

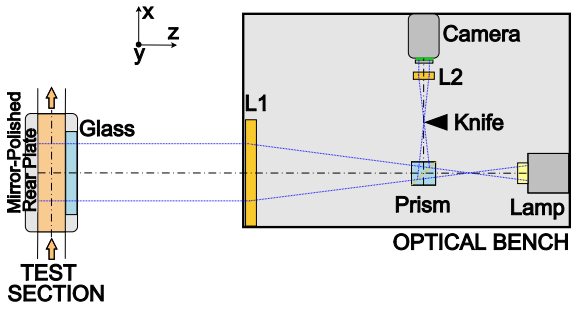

Figure 3. Schematical representation of the optical bench used for schlieren visualizations.

White light rays from a 100 W mercury vapor lamp are collimated by a bi-convex lens (L1, $f_1 = 1000\ mm$, $d_1 = 150\ mm$) and enter the test section perpendicularly to it. They are deflected by density gradients in the fluid flow and are reflected back by the mirror-finished rear steel plate. The reflected beams cross the test section again and are focused by lens L1 (which therefore also constitutes the schlieren head) at the knife edge, after a 90° rotation operated by a beam splitter cube. The schlieren image is then formed onto the sensor of a high-speed CMOS camera by a second lens (L2, $f_2 = 75\ mm$, $d_2 = 52\ mm$). The distance between components is determined from the fundamental law of optical geometry for thin lenses [8].
In order to visualize the horizontal density gradients along the nozzle axis, the knife is set in the vertical direction. Positive density gradients (compressions and shock waves) should appear dark whilst negative density gradients (expansions and expansion fans) should appear bright [9].

EXPERIMENTAL RESULTS

Measuring Range Issues

Schlieren images show measuring range issues in the throat region of nozzle MDM_{M2}, where expansion fans caused by the presence of the recessed step appear as dark instead of being bright (Figure 2). This was attributed to the strong density gradients occurring in non-ideal flows of MDM, causing refractions intense enough to deflect light onto some system aperture stop. In order to verify this hypothesis, ray tracing calculation was performed. The calculation procedure, not reported here for brevity, involved tracking light rays through the optical bench apparatus with a lumped parameters approach. Ray deflection across the fluid flow was calculated as $\varepsilon = \frac{L}{n_\infty} K \frac{d\rho}{dx}$ [9,10]; Snell's law was employed at interfaces of homogeneous media and the Ray Transfer Matrix approach was used to determine ray deviations across thin lenses [8]. Figure 4 is an example of the output of the purposely written *Matlab*® code, showing which modelled rays do not reach the sensor. Analogous plots were drawn for each component in the optical system before the sensor, so that the rays blocked by each element were identified by comparison of the plots of a component and the preceding one. This analysis indicated that rays crossing regions of the test area with stronger density gradients were deviated so much as to be intercepted by the knife frame before reaching the camera sensor.

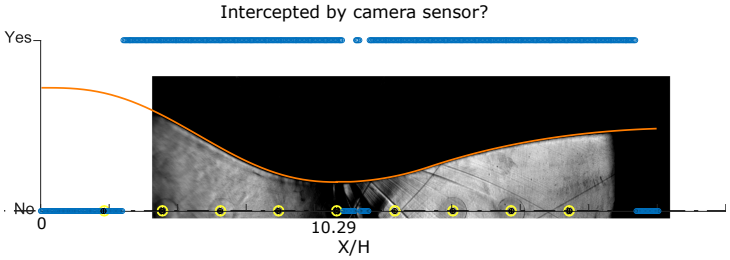

Figure 4. Ray tracing output for Test 04, MDM_a, $Z_T = 0.82$. The figure is a scatter plot of the initial ray x-coordinates along the nozzle axis, indicating whether they reach the camera sensor or not. Light rays coming from expansion fans are indeed blocked in their path by the knife frame before reaching the camera sensor.

As the test proceeds (so, as total pressure decreases and the stagnation compressibility factor Z_T increases), measuring range issues are reduced: the expansion fans become less dark, until they eventually become bright (as they should always be) as shown in Figure 5. Also, when the same nozzle geometry was used for testing with air, measuring range issues were much less noticeable or even not present at all.

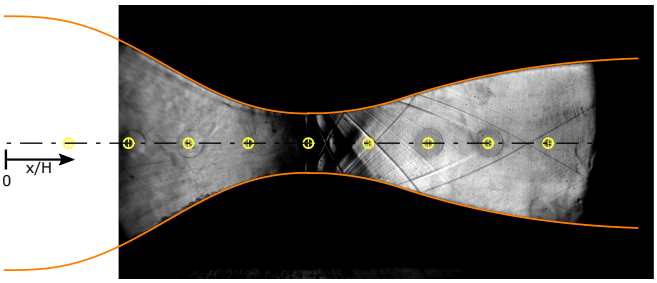

(a) MDM_a, $Z_T = 0.82$

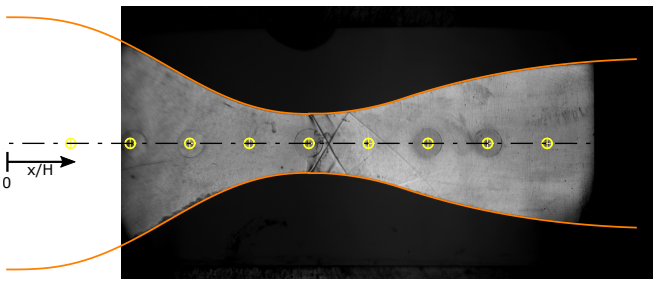

(b) MDM_e, $Z_T = 0.97$

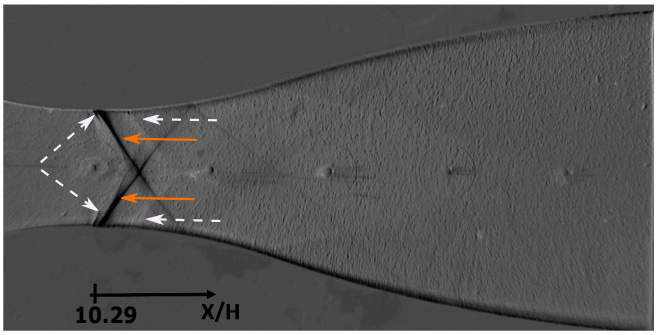

(c) Air - image from 7

Figure 5. Schlieren images of *Test04* with MDM for minimum a) and maximum b) Z_T values and for air c). Measuring range issues associated with expansion fans evidently decrease for MDM as Z_T increases and are much less noticeable for air compared to all MDM conditions (expansion fans are almost completely bright).

Refractive Index Gradient

The schlieren technique is sensitive to the refractive index gradient along the nozzle axis (x-direction), therefore this quantity is investigated to explain the discussed measuring range issues. Since the latter extend to the axis (Figure 5), the analysis is performed at the axis only.

If the Gladstone-Dale relation ($n = 1 + K\rho$) is valid and K is constant along the x-direction, as it is the case in both air and MDM flows investigated, then:

$$\frac{\partial n}{\partial x} = K \frac{\partial \rho}{\partial x} \tag{1}$$

This expression was used to calculate the refractive index gradient (shown in Figure 6) for all examined conditions starting from CFD simulations. Results were extracted from the axis line of viscous 2D CFD simulations having the same stagnation conditions and nozzle geometry as experimental tests, and employing the full Reynolds-averaged compressible Navier-Stokes equations for non-ideal compressible turbulent flows. CFD results were employed in the present analysis instead of experimental measures (standing the excellent accordance between the two sets of data [12]) because of their much finer spatial discretization, making them more suitable for the accurate evaluation of the local density gradients along the nozzle axis to explain the observed schlieren images.

For air, K was calculated from reference conditions (0) as $K = (n_0 - 1)\frac{T_0}{P_0}\frac{\mathcal{R}}{M_m}$ thanks to the Polytropic Ideal Gas (PIG) assumption, resulting in $K_{air} = 2.27 \cdot 10^{-4}\ m^3/kg$. For MDM, the Gladstone-Dale relation was assumed as valid too, because the $n(\rho)$ relation determined with the Lorentz-Lorentz relation (using liquid reference data and the assumption of constant molar refractivity, see [13]) showed an almost perfectly linear trend. K_{MDM} was determined as the slope of the interpolating line, and was found to be $K_{MDM} = 4.30 \cdot 10^{-4}\ m^3/kg$.

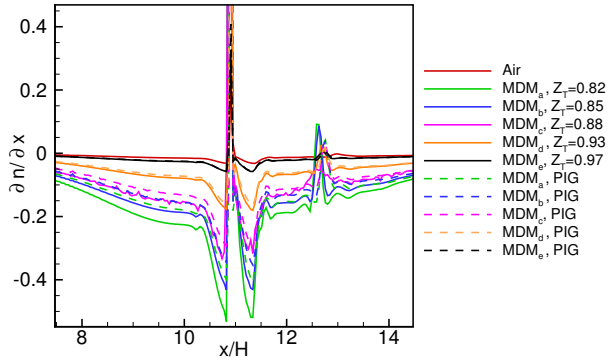

Figure 6. Refractive index gradient at the throat of nozzle MDM_{M2} for all MDM and air conditions (solid lines). PIG simulations are also shown as dashed lines.

For an isentropic process (like the considered flow at the nozzle axis) the refractive index gradient can be conveniently rewritten highlighting the compressibility ($1/c^2$) and the pressure ratio along the nozzle, as:

$$\frac{\partial n}{\partial x} = K \frac{1}{c^2} P_T \frac{\partial (P/P_T)}{\partial x} \tag{2}$$

The following analysis proceeds in two steps: the polytropic ideal gas (PIG) model is first employed and then real gas effects are introduced.

For a PIG, the speed of sound is:

$$c = \sqrt{\gamma \frac{\mathcal{R}}{M_m} T_T \left(1 + \frac{\gamma - 1}{2} M^2\right)^{-1}} \tag{3}$$

If the PIG fluid and the geometry are fixed, all quantities are determined except for total conditions: they are thus the only changing parameters determining the intensity of $\frac{\partial n}{\partial x}$.
If the same geometry but different PIGs are compared, the different values of compressibility and of the Gladstone-Dale constant also determine the refractive index gradient. From ideal gas theory, the most dominant factor determining speed of sound (and thus, $1/c^2$) is molar mass [11]. Conversely, M_m does not affect the Mach number and pressure ratio trends. CFD simulations of fluids with different values of γ but the same MDM_{M2} geometry (not reported here for brevity) show that the Mach number and pressure ratio trends are almost coincident in the throat region, so they yield negligible contribution to the difference in refractive index gradient between fluids. The Gladstone-Dale constant can significantly vary for different fluids, and, in the case of a PIG, can be calculated from reference conditions (0) analogously to air.
In case of a real gas, the need for a more complex thermodynamic model makes it impossible to employ a simple expression for c and thus draw straightforward conclusions. Therefore, real gas effects on the refractive index gradient are analysed by comparing CFD simulations of real MDM flows at every Z_T (Table 1) to the respective PIG MDM flows (characterized by $\gamma = 1.018$). Total conditions and the Gladstone-Dale coefficient are equal for real and PIG simulations at each Z_T. The direct and explicit impact of these variables is thus eliminated and differences in the refractive index gradients between real and ideal cases (shown in Figure 6) can be attributed to real gas effects only. The latter implicitly depend on total inlet conditions and have an impact on the pressure ratio gradient and on compressibility. Real gas effects are responsible for weak quantitative differences in pressure ratio gradients between real and PIG simulations (not shown here for brevity), yielding limited contribution to the difference in their respective refractive index gradients. Instead, real gas effects have a significant impact on the speed of sound and, thus, on quantity $1/c^2$. The speed of sound for PIG simulations monotonically decreases along the expansion, consistently with the PIG hypothesis, whilst non-ideal gas effects determine an increase in the speed of sound along the expansion [14]. Moreover, flow non-idealities can determine an increase or a decrease in the value of c with respect to the PIG model, depending on the intensity of attractive and repulsive forces [15, 16]. Conditions in Test04 are such that the value of c for the real flow is lower than for the respective PIG; as a consequence, the parameter $1/c^2$ for the real gas is larger, as seen in Figure 7, determining a stronger refractive index gradient (Figure 6) compared to the corresponding PIG model. As the flow becomes more ideal, the trend in c flattens and tends towards the one of its corresponding PIG. This is why the difference between real MDM refractive index gradient and the respective PIG one reduces as Z_T increases (Figure 6). If the different real flows are compared to one another, quantity $1/c^2$ is always larger at lower values of Z_T (Figure 7) in the throat region due to stronger real gas effects, contributing to a stronger refractive index gradient there (Figure 6).

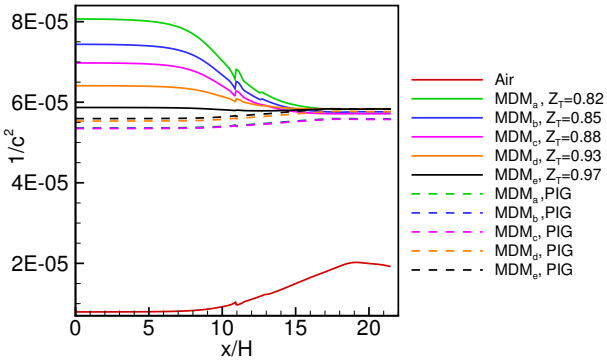

Figure 7. Compressibility $1/c^2$ along the nozzle axis for all MDM test conditions (real and ideal) and for air.

To summarize, the analysis of parameters in Equation 2 for the refractive index gradient provides an explanation for the trends in measuring range issues. If real MDM flows at different Z_T are compared, total conditions play a direct role in determining the refractive index gradient through the value of P_T and also have an indirect impact because they determine the extent of real gas effects. The latter only weakly affect the pressure ratio gradient, but make compressibility in the throat region larger as Z_T decreases, in the case of the MDM flows analyzed in this work. From MDM_a to MDM_e conditions, compressibility changes by a factor lower than 2, whilst total pressure changes by a factor larger than 7 (Table 1). It can therefore be concluded that, although real gas effects do have an impact, the most important parameter in determining the different values of the refractive index gradient, and thus, the extent of the measuring range issues during the test, is total pressure.
Comparison between MDM and air flows needs to be taken into steps: polytropic ideal gases are first considered, and real gas effects are then added on. If CFD simulations of air and MDM with the polytropic ideal gas model are compared, it is evident that, referring to Equation 2, the pressure ratio gradient in the throat region is only weakly affected by molecular complexity. Also, air's speed of sound is more than two times MDM's: compressibility for MDM-PIG is thus more than four times air's (Figure 7), contributing to stronger refractive index gradients in MDM. Due to real gas effects, the speed of sound for a real MDM flow is lower than the respective PIG, so even lower than air. The value of $1/c^2$ for air is therefore much lower than for a real MDM flow (by a factor of about 6), due to the combined impact of molecular complexity, molecular mass, temperature (weak) and real gas effects. It must also be pointed out that the Gladstone-Dale coefficient for MDM is almost twice that of air, yielding another contribution to the stronger $\frac{\partial n}{\partial x}$ for MDM. Therefore, a much lower compressibility, together with the lower value of the Gladstone-Dale coefficient, leads to less intense refractive index gradients (Figure 6) and measuring issues for air than all real MDM flows (compare images for MDM and air in Figure 5).

CONCLUSIONS

The present paper looked at the measuring range issues associated with schlieren visualizations of a non-ideal flow of Siloxane MDM in a converging-diverging nozzle representative of flows in ORC turbines. The presence of a recessed step at the throat is responsible for the existance of an oblique shock wave and two expansion fans. The latter, in particular, appear as dark regions in the schlieren image instead of being bright. Ray tracing calculation revealed that density gradients cause a refraction so intense as to deviate light rays onto the knife frame, thus preventing them from reaching the sensor. Interestingly, this measuring range issue was observed to decrease as the non-ideality of the flow decreased. Moreover, when the same geometry was employed for preliminary testing with air, this issue was almost non-existant.
In the attempt of explaining these two observations, the present discussion derived an analytical expression for the refractive index gradient. The impact of each identified parameter was investigated with the use of CFD simulations, first for a polytropic ideal gas and then for a real gas, to particularly highlight the role of real gas effects in the value of the refractive index gradient, and thus, on the extent of measuring range issues.
Total conditions were found to be the most important variable in the value of the refractive index gradient when MDM flows with different degrees of non-ideality were compared. They had both a direct impact as well as an indirect one, by determining the extent of real gas effects and thus the value of compressibility. When air and MDM flows at every inlet condition were compared, the very different value of compressibility (both due to the different molecular mass and real gas effects) and of the Gladstone-Dale constant were found to determine a lower refractive index gradient for the latter fluid, and thus, less intense or almost absent measuring range issues.

REFERENCES

[1] P. Colonna, E. Casati, C.Trapp, T. Mathijsen, J. Larjola, T.Turunen-Saaresti, A. Uusitalo, Organic Rankine Cycle Power Systems: from the concept to current technology, applications and an outlook to the future, *Journal of Engineering for Gas Turbines and Power, ASME*, Vol. 137, October 2015.

[2] E. Macchi and M. Astolfi, Organic Rsnkine Cycle (ORC) Power Systems. Technologies and applications, Woodhead Publishing Series in Energy: Number 107, Elsevier, 2017.

[3] Spinelli, A., Pini, M., Dossena, V., Gaetani, P. and Casella, F.,Design, Simulation, and Construction of a Test Rig for Organic Vapours,*ASME Journal of Engineering for Gas Turbines and Power*, Vol.135, Pages 042303, 2013.

[4] Guardone, A., Spinelli, A. and Dossena, V., Influence of Molecular Complexity on Nozzle Design for an Organic Vapor Wind Tunnel, *ASME Journal of Engineering for Gas Turbines and Power*, Vol. 135, Pages 042307, 2013.

[5] R. Span and W. Wagner, Equations of State for Technical Applications. I. Simultaneously Optimized Functional Forms for Nonpolar and Polar Fluids. *Int. J. Thermophys.*, Vol. 24, Pages 1-39, January 2003.

[6] P. Colonna and T. P. van der Stelt, FluidProp: a program for the estimation of thermo physical properties of fluids, Software, http://www.FluidProp.com, 2004.

[7] Spinelli, A. and Guardone, A. and Cozzi, F. and Carmine, and Cheli, R. and Zocca, M. and Gaetani, P. and Dossena, V., Experimental Observation of Non-ideal Nozzle Flow of Siloxane Vapor MDM, *3rd International Seminar on ORC Power Systems*, 103; 2015.

[8] G. Chartier, Introduction to Optics, Springer, 2005.

[9] G. S. Settles, Schlieren and Shadowgraph techniques. Visualizing Phenomena in Transparent Media, Springer, 2001.

[10] W. Merzkirch, Flow Visualization, Academic Press, 1987.

[11] P. A. Thompson, Compressilbe Fluid Dynamics, McGraw-Hill, New York, NY, 1988.

[12] G. Gori, M. Zocca, G. Cammi, A. Spinelli and A. Guardone, Experimental Assessment of the open-source SU2 CFD suite for ORC applications, *Accepted for publication in Proceedings of the 4th International Seminar on ORC Power Systems, Milan*, September 2017.

[13] Liu, Y. and Daum, P.H., Relationship of Refractive Index to Mass Density and Self-consistency of Mixing Rules for Multicomponent Mixtures Like Ambient Aerosols, *Journal of Aerosol Science*, N. 39, Pages 974-986, 2008.

[14] P. A. Thompson, A fundamental derivative in gas dynamics, *Phys. Fluids*, Vol. 14, Pages 1843-1849, 1971.

[15] J. Harinck and A. Guardone and P. Colonna, The influence of molecular complexity on expanding flows of ideal and dense gases, *Phys. of Fluids*, Vol. 21, Pages 086101, 1-14, August 2009.

[16] P. Colonna and A. Guardone, Molecular interpretation of nonclassical gas dynamics of dense vapors under van der Waals model, *Phys. of Fluids*, Vol. 18, Pages 056101, 1-14, May 2006.